

Andreev-Fano Effect in a Hybrid Normal-Metal / Superconductor Interferometer

Yu Zhu¹, Qing-feng Sun², and Tsung-han Lin^{1*}

*State Key Laboratory for Mesoscopic Physics and
Department of Physics, Peking University, Beijing
100871, China¹*

*Center for the Physics of Materials and
Department of Physics, McGill University, Montreal,
PQ, Canada H3A 2T8²*

()

Abstract

We report on a new type of Fano effect, named as Andreev-Fano effect, in a hybrid normal-metal / superconductor (N/S) interferometer embedded with a quantum dot. Compared with the conventional Fano effect, Andreev-Fano effect has some new features related to the characteristics of Andreev reflection. In the linear response regime, the line shape is the square of the conventional Fano shape; while in the nonlinear transport, a sharp resonant structure is superposed on an expanded interference pattern, qualitatively different from the conventional Fano effect. The phase dependence of the hybrid N/S interferometer is also distinguished from those of all-N or all-S interferometers.

PACS numbers: 74.50.+r, 73.63.Kv, 85.35.Ds, 73.23.-b

When a resonant channel interferes with a nonresonant channel, the line shape of the resonance will change into an asymmetric one, sometimes even become to an antiresonance. This phenomenon is known as Fano effect [1], which has been recognized in a large variety of systems, such as atomic photoionization, electron and neutron scattering, Raman scattering, and photoabsorption in quantum well structures, etc. Recently, the effect is observed in the electron transport through mesoscopic systems. Several groups reported Fano resonance in spectroscopic measurements of a single magnetic adatom absorbed on the surface of normal metal, using scanning tunneling microscope [2,3,4,5]. The results can be well understood by generalizing the noninteracting resonant channel in the original Fano problem to the many-body Kondo resonance [6,7,8]. Meanwhile, Fano resonance is also reported in the conductance through a single electron transistor fabricated in semiconductor [9], which has the advantage that the key parameters are experimentally controllable.

Another active field in recent years is the so called “mesoscopic superconductivity”, which has been greatly advanced with the progress of nanofabrication technology [10]. Adding superconducting materials to the conventional mesoscopic systems changes the coherent transport through the hybrid system significantly. At the interface of normal-metal (N) and superconductor (S), a two-particle process called Andreev reflection (AR) plays an essential role in the subgap conductance, in which an electron is reflected as a hole in the N side, and a Cooper pair is created in the S side [11]. Many new effects involving AR are investigated both experimentally and theoretically (for a recent review see [12]).

What will occur if one of the electrodes in the mesoscopic Fano system is replaced by a superconductor? Let us consider a N/S hybrid interferometer, one arm contains a point contact with tunable conductance, the other arm is embedded with a quantum dot (QD) with resonant levels. The proposed structure is schematically shown in Fig.1, and hereafter is referred to as N-(I,QD)-S. The conductance through the path N-I-S provides a nonresonant channel, and the transport properties have been studied in [13,14]. While the conductance through the path N-QD-S provides a resonant channel, and the transport properties have been studied in [15,16]. The interplay of the two channels in N-(I,QD)-S are double folded: interference between resonant AR and nonresonant AR, and opening up a new conducting channel, named as cross AR. Due to the interference among these AR processes, we find a new type of Fano effect, named as Andreev-Fano effect, which has distinct features compared with the conventional Fano effect. In the linear response regime, the line shape is the square of the conventional Fano shape; while in the nonlinear transport, a sharp resonant structure

is superposed on an expanded interference pattern. The phase dependence of the hybrid N/S interferometer is also distinguished from those of all-N or all-S interferometers.

The N-(I,QD)-S structure is modelled by the Hamiltonian

$$H = H_L + H_R + H_{dot} + H_T , \quad (1)$$

where $H_L = \sum_{k\sigma} \varepsilon_{Lk} a_{Lk\sigma}^\dagger a_{Lk\sigma}$ is for the left N electrode, $H_R = \sum_{k\sigma} \varepsilon_{Rk} a_{Rk\sigma}^\dagger a_{Rk\sigma} + \sum_k (\Delta a_{Rk\uparrow}^\dagger a_{R-k\downarrow}^\dagger + H.c.)$ is for the right S electrode, $H_{dot} = \sum_{\sigma} E_0 c_{\sigma}^\dagger c_{\sigma}$ is for the QD embedded in one arm of the interferometer, and $H_T = t_L \sum_{k\sigma} a_{Lk\sigma}^\dagger c_{\sigma} + t_R \sum_{k\sigma} a_{Rk\sigma}^\dagger c_{\sigma} + w \sum_{kk'} a_{Lk\sigma}^\dagger a_{Rk'\sigma} + H.c.$ is for the phase coherent tunneling within the interferometer.

To proceed, we introduce the following Green function matrix

$$\mathbf{G} \equiv \langle\langle \begin{pmatrix} C \\ A_L \\ A_R \end{pmatrix} | \begin{pmatrix} C^\dagger & A_L^\dagger & A_R^\dagger \end{pmatrix} \rangle\rangle = \begin{pmatrix} G_{DD} & G_{DL} & G_{DR} \\ G_{LD} & G_{LL} & G_{LR} \\ G_{RD} & G_{RL} & G_{RR} \end{pmatrix} , \quad (2)$$

in which

$$C = \begin{pmatrix} c_\uparrow \\ c_\downarrow^\dagger \end{pmatrix}, \quad A_L = \begin{pmatrix} \sum_k a_{Lk\uparrow} \\ \sum_k a_{L-k\downarrow}^\dagger \end{pmatrix}, \quad A_R = \begin{pmatrix} \sum_k a_{Rk\uparrow} \\ \sum_k a_{R-k\downarrow}^\dagger \end{pmatrix} . \quad (3)$$

One can write down the Dyson equation of the system as $\mathbf{G} = \mathbf{g} + \mathbf{g}\mathbf{\Sigma}\mathbf{G}$, with \mathbf{g} being the decoupled Green function in the limit of $H_T \rightarrow 0$, and $\mathbf{\Sigma}$ being the self-energy arise from the coherent tunneling. The corresponding Dyson equation for \mathbf{G}^r and Keldysh equation for $\mathbf{G}^<$ read

$$\mathbf{G}^r = (\mathbf{g}^{r-1} - \mathbf{\Sigma})^{-1} , \quad (4)$$

$$\mathbf{G}^< = \mathbf{G}^r \mathbf{g}^{r-1} \mathbf{g}^< \mathbf{g}^{a-1} \mathbf{G}^a , \quad (5)$$

in which $\mathbf{\Sigma} = \mathbf{\Sigma}^a = \mathbf{\Sigma}^r$ is the matrix of tunneling elements.

The current flowing out of the electrode β can be expressed in term of these Green functions,

$$I_{\beta\sigma} = \frac{e}{\hbar} 2 \text{Re} \int \frac{d\omega}{2\pi} \text{Tr} [\mathbf{Q}_{\beta\sigma} \mathbf{\Sigma} \mathbf{G}^<], \quad (\beta = L, R) \quad (6)$$

in which

$$\mathbf{Q}_{L\sigma} = \begin{pmatrix} 0 & & \\ & q_\sigma & \\ & & 0 \end{pmatrix}, \quad \mathbf{Q}_{R\sigma} = \begin{pmatrix} 0 & & \\ & 0 & \\ & & q_\sigma \end{pmatrix}, \quad (7)$$

$$q_\uparrow = \begin{pmatrix} 1 & 0 \\ 0 & 0 \end{pmatrix}, \quad q_\downarrow = \begin{pmatrix} 0 & 0 \\ 0 & -1 \end{pmatrix}, \quad (8)$$

are matrices with element +1 for electron and -1 for hole. For the non-spin-polarized case considered in this paper, the total current through the interferometer is $I = I_{L\uparrow} + I_{L\downarrow} = 2I_{L\uparrow}$. The current can be separated into two parts: the AR current I_A and the conventional tunneling current I_B ,

$$I_A = \frac{2e}{\hbar} \int \frac{d\omega}{2\pi} T_A(\omega) [f(\omega - eV) - f(\omega + eV)] \quad , \quad (9)$$

$$I_B = \frac{2e}{\hbar} \int \frac{d\omega}{2\pi} T_B(\omega) [f(\omega - eV) - f(\omega)] \quad . \quad (10)$$

It can be shown that $T_B(\omega)$ contains a factor $\frac{|\omega|}{\sqrt{\omega^2 - \Delta^2}} \theta(|\omega| - \Delta)$, and therefore is negligible when $|eV| < \Delta$. $T_A(\omega)$ is derived as

$$T_A(\omega) = 2 \operatorname{Re} \operatorname{Tr} \left[\mathbf{Q}_{L\uparrow} \Sigma \mathbf{G}^r \mathbf{Q}_{L\downarrow} (\mathbf{g}^{r^{-1}} - \mathbf{g}^{a^{-1}}) \mathbf{G}^a \right] \quad . \quad (11)$$

Since we are concerning the subgap conductance where AR dominates, we take the limit $\Delta \rightarrow \infty$ in the evaluation of $T_A(\omega)$. After some algebra, $T_A(\omega)$ can be explicitly obtained as

$$T_A(\omega) = \frac{\left| \frac{1}{2}LR - 2\sqrt{xL\overline{R}}E_0 e^{i\phi} - 2x(\omega^2 - E_0^2)e^{i2\phi} \right|^2}{\left[(1+x^2)(\omega^2 - E_0^2) - \frac{L^2+R^2}{4} + 2x\sqrt{xL\overline{R}}E_0 \cos \phi - xLR \cos^2 \phi \right]^2 + [(L+xR)\omega]^2} \quad (12)$$

where $L \equiv 2\pi N_L |t_L|^2$, $R \equiv 2\pi N_R |t_R|^2$, and $x \equiv \pi^2 N_L N_R |w|^2$ are the coupling strengths among N, S, and QD, with N_L and N_R being the density of states in the left and right electrodes. ϕ is the Aharonov-Bohm (AB) phase induced by a magnetic flux. It can be shown that $0 \leq T_A(\omega) \leq 1$ as required by the physical meaning of transmission probability. Specially, if $x \rightarrow 0$, $T_A(\omega) = \frac{1}{4}L^2 R^2 / \left[(\omega^2 - E_0^2 - \frac{L^2+R^2}{4})^2 + L^2 \omega^2 \right]$ reproduces the transmission probability of N-QD-S; if $L \rightarrow 0$ and $R \rightarrow 0$, $T_A(\omega) = \frac{4x^2}{(1+x^2)^2}$ reproduces the transmission probability of N-I-S.

At zero temperature and in the subgap regime, the total current is reduced to $I = \frac{2e}{\hbar} \int_{-eV}^{eV} \frac{d\omega}{2\pi} T_A(\omega)$. The integral can be evaluated analytically in two limits: linear response

regime where $eV \rightarrow 0$ and strong nonlinear regime where $eV \rightarrow \infty$ [17]. For $eV \rightarrow 0$, the conductance at zero bias is

$$G_0 \equiv \lim_{V \rightarrow 0} \frac{I(V)}{V} = \frac{4e^2}{h} T_b \left[\frac{\left(E_0 - \frac{\sqrt{xLR}}{2x} \cos \phi\right)^2 + \frac{LR}{4x} \sin^2 \phi}{\left(E_0 - \frac{x\sqrt{xLR}}{1+x^2} \cos \phi\right)^2 + \frac{xLR}{(1+x^2)^2} \cos^2 \phi + \frac{L^2+R^2}{4(1+x^2)}} \right]^2, \quad (13)$$

in which $T_b \equiv \frac{4x^2}{(1+x^2)^2}$ is the transmission probability through the arm of N-I-S. For $eV \rightarrow \infty$, the net current in high voltage limit is

$$\begin{aligned} I_\infty &\equiv \lim_{V \rightarrow \infty} \left[I(V) - \frac{4e^2}{h} T_b V \right] \\ &= \frac{2e}{h} \frac{2}{(L+xR)(1+x^2)} \left[xLR \sin^2 \phi - \frac{x^2}{(1+x^2)^2} (L+xR)^2 \right. \\ &\quad \left. + \frac{\left(\frac{1-x^2}{1+x^2} \sqrt{xLR} \cos \phi E_0 + \frac{x^2}{1+x^2} LR \cos^2 \phi + \frac{x(L^2+R^2)}{4(1+x^2)} - \frac{LR}{4}\right)^2}{\left(E_0 - \frac{x\sqrt{xLR}}{1+x^2} \cos \phi\right)^2 + \frac{xLR \cos^2 \phi}{(1+x^2)^2} + \frac{L^2+R^2}{4(1+x^2)}} \right], \end{aligned} \quad (14)$$

in which the background current through the arm of N-I-S has been subtracted from the total current for convergence.

Equation (12), (13), and (14) are the central results of this paper, which describe the Andreev-Fano effect in the N-(I,QD)-S structure. Below we shall discuss in detail the physical meaning of these results by numerical calculation.

Fig.2 shows the curves of net conductance $G \equiv G_0 - \frac{4e^2}{h} T_b$ at zero bias voltage and the net current $I \equiv I(V) - \frac{4e^2}{h} T_b V$ at finite voltages for vanishing AB phase, with $\sqrt{L^2+R^2} \equiv 1$ as energy unit. For comparison, the corresponding curves in N-(I,QD)-N are also shown in the plot, where the background conductance $\frac{4e^2}{h} T_b$ should be replaced by $\frac{2e^2}{h} T'_b$ with $T'_b = \frac{4x}{(1+x)^2}$, and the energy unit replaced by $(L+R)/(1+x)$. The background conductance $\frac{4e^2}{h} T_b$ is contributed by the transport through the arm N-I-S, while the net conductance (current) is contributed by remaining conducting paths and the interference among all channels. The interference is so important in the coherent transport that the net conductance (current) could even be negative. In the linear response regime, one can see in the plot that the pattern of conventional Fano effect and Andreev-Fano effect are analogous. With the increase of background conductance, the original resonant peak becomes asymmetric, then evolves into a positive and a negative peak, finally into an antiresonance which is the result of destructive interference. Despite of the similarity, the line shapes are different: the conventional Fano effect has the shape of $\frac{1}{1+q^2} \frac{(\varepsilon+q)^2}{\varepsilon^2+1}$ while the Andreev-Fano effect has $\left[\frac{1}{1+q^2} \frac{(\varepsilon+q)^2}{\varepsilon^2+1} \right]^2$, where ε is the effective resonant level and q the Fano parameter.

At finite voltages, the conventional Fano effect and the Andreev-Fano effect are qualitatively different, which is apparent by comparing (a3) with (b2) in Fig.2. In conventional Fano effect, the resonant structure at zero bias voltage is pulled to a flat ridge or valley by finite voltages, while in Andreev-Fano effect, the resonant structure near $E_0 = \mu_R$ remains sharp even in the high voltage limit, and the resonance reverses its sign from positive to negative then return to positive with the increase of background conductance. In addition, the sharp resonant structure is superposed on an expanded interference pattern in the range of $eV < |E_0 - \mu_R|$. These differences stem from the different conducting mechanisms. In N-(I,QD)-N, electron transport is dominated by the single particle process. The N-QD-N arm becomes conductive when the resonant level E_0 is within the chemical potentials of the left and right N electrodes. Therefore, the interference pattern is simply expanded to the ranges of $\mu_L < E_0 < \mu_R$ by the finite voltages. In N-(I,QD)-S, on the contrast, electron transport in the subgap regime is governed by AR. There are three types of AR in the N-(I,QD)-S system (see fig.1), (a) resonant AR through the path N-QD-S, (b) non-resonant AR through the path N-I-S, and (c) cross AR with the incident electron coming from N-QD-S and the reflected hole going through N-I-S. The features of Andreev-Fano effect at finite voltages can be well interpreted with the these AR processes. When $|E_0 - \mu_R| > eV$, only process (b) is allowed, resulting in a flat background current. So the net current $I \rightarrow 0$ after subtracting the background. When $eV > |E_0 - \mu_R| > O(1)\sqrt{L^2 + R^2}$, process (b) and (c) are active, their interference lead to a current pattern similar to that of N-(I,QD)-N. When $|E_0 - \mu_R| < O(1)\sqrt{L^2 + R^2}$, the conducting channel (c) is open. (Notice that resonant AR occurs only when the resonant level lines up with the chemical potential of S, because both the incident electron and the reflected hole have to pass QD through the resonant level.) Consequently, a resonant structure is superposed on the former interference pattern. The interference among (a), (b), and (c) makes the resonant peak reverse its sign twice. For a quantitative analysis, let us consider I_∞ at $\phi = 0$. The current formula can be formally rewritten to a conventional Fano shape $I_\infty = A_1 + A_2 \frac{(\varepsilon+q)^2}{\varepsilon^2+1}$, in which

$$q = \frac{2x\sqrt{xLR} + \frac{1+x^2}{1-x^2} \frac{x(L^2+R^2)+LR(3x^2-1)}{2\sqrt{xLR}}}{\sqrt{(L+xR)^2 + (R+xL)^2}}$$

is the effective Fano parameter of the resonant peak. Obviously, $q \rightarrow -\infty$ if $T_b \rightarrow 0$, $q \rightarrow +\infty$ if $T_b \rightarrow 1$, and $q = 0$ at some intermediate T_b , which are corresponding to the sign reverse of the resonant peak.

Next, we investigate the phase dependence of the hybrid N/S interferometer. Notice

that the current has the following features: $I(\phi + 2\pi) = I(\phi)$ due to the general property of AB rings, $I(\pi - \phi, -E_0) = I(\phi, E_0)$ due to particle and hole symmetry, and $I(-\phi) = I(\phi)$ analogous to the phase locking effect in conventional two-terminal structures [18] but here the conducting mechanism is AR. The left panel of Fig.3 shows the curves of G vs E_0 at zero bias voltage and I vs E_0 at finite voltages, with T_b fixed at 0.5 and ϕ chosen as 0, $\frac{\pi}{4}$, and $\frac{\pi}{2}$. (Only the cases of $0 \leq \phi \leq \frac{\pi}{2}$ are shown due to the features of $I(\phi)$.) In the linear response regime, the interference pattern evolves from asymmetric to symmetric shape when ϕ changes from 0 to $\frac{\pi}{2}$, but the dependence on ϕ is insensitive. At finite voltages, however, the pattern exhibits a strong dependence on ϕ . Especially, the current platform in the high voltage limit oscillates with ϕ according to $-\frac{e}{\hbar} \frac{LR}{L+xR} T_b^{3/2} \cos 2\phi$. The right panel of fig.3 shows the curves of G vs ϕ and I vs ϕ at selected points marked in the left curves. In the linear response regime, the phase dependence is dominated by $\cos \phi$ or $\cos(\phi + \pi)$ component with an abrupt π phase shift around $E_0 = \mu_R$. While in the high voltage limit the phase dependence is dominated by $\cos 2\phi$ component without any abrupt phase shift. At intermediate voltages, the phase dependence is much more complicated: $\cos \phi$ and $\cos(\phi + \pi)$ dominate in the range of $E_0 - \mu_R < -eV$ and $E_0 - \mu_R > eV$, respectively; $\cos \phi$ and $\cos 2\phi$ coexist in the range of $-eV < E_0 - \mu_R < 0$; $\cos(\phi + \pi)$ and $\cos 2\phi$ coexist in the range of $0 < E_0 - \mu_R < eV$; both $\cos \phi$ and $\cos(\phi + \pi)$ vanish around $E_0 = \mu_R$ and only $\cos 2\phi$ dominates there. Despite of the constraint of the phase locking, our results suggest that more information could be extracted from the analysis of higher harmonics $\cos 2\phi$. The results share some similarity with the phase dependence of Kondo-Fano effect studied in [8]. The coexistence of $\cos \phi$ and $\cos 2\phi$ harmonics in the hybrid N/S interferometer is can be understood as follows. Taking account of various AR processes and considering only the direct trajectory, the transmission probability through the interferometer is $\left| t_{1\uparrow} t_{1\downarrow} + t_{2\uparrow} e^{i\phi} t_{2\downarrow} e^{i\phi} + t_{1\uparrow} t_{2\downarrow} e^{i\phi} + t_{1\downarrow} t_{2\uparrow} e^{i\phi} \right|^2$, in which $t_{1\sigma}$ ($t_{2\sigma}$) is the tunneling amplitude through the upper (lower) arm. Both $\cos \phi$ and $\cos 2\phi$ emerge in the interference terms. One can see in Eq.(12) that the numerator of $T_A(\omega)$ is just of this form, while the additional $\cos \phi$ and $\cos^2 \phi$ terms in the denominator can be attributed to the trajectory with higher winding number.

To sum up, we have reported the Andreev-Fano effect in a hybrid N/S interferometer, and found some new features compared with the conventional Fano effect. Both the interference pattern and the phase dependence of the hybrid N/S interferometer are different to the conventional all-N or all-S interferometer, which originates from different conducting mechanism. We believe that the proposed structure can be achieved with the available

technique, e.g., replacing the N-tip of scanning tunneling microscope by a S-tip in the mesoscopic Fano system [2,3,4,5], or modifying the structure of the Andreev interferometer in the experiment [19], or fabricating the design in the S-2DEG hybrid systems [20], etc. We are looking forward to hearing the relevant experimental response.

The authors would like to thank Z. S. Ma for stimulating discussion. This project was supported by NSFC under Grants No. 10074001 and No. 90103027, and also by the Visiting Scholar Foundation of State Key Laboratory for Mesoscopic Physics in Peking University.

* To whom correspondence should be addressed.

REFERENCES

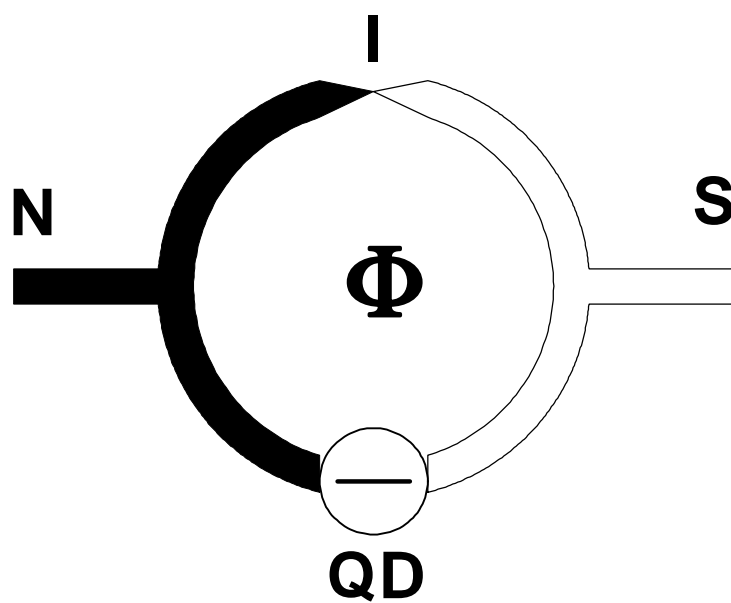
- [1] U. Fano, Phys. Rev. **124**, 1866 (1961).
- [2] V. Madhavan *et al.*, Science **280**, 567 (1998).
- [3] J. Li *et al.*, Phys. Rev. Lett. **80**, 2893 (1998).
- [4] H. C. Manoharan, C. P. Lutz, and D. M. Eigler, Nature (London) **403**, 512 (2000).
- [5] N. Knorr *et al.*, Phys. Rev. Lett. **88**, 096804 (2002).
- [6] A. Schiller and S. Hershfield, Phys. Rev. B. **61**, 9036 (2000).
- [7] O. Újsághy *et al.*, Phys. Rev. Lett. **80**, 2893 (1998).
- [8] W. Hofstetter, J. König, and H. Schoeller, Phys. Rev. Lett. **87**, 156803 (2001).
- [9] J. Göres *et al.*, Phys. Rev. B **62**, 2188 (2000).
- [10] *Proceeding of Mesoscopic Superconductivity*, Physica C **352**, p1-233 (2001), edited by H. Takayanagi and T. Claeson.
- [11] A. F. Andreev, Zh. Eksp. Teor. Fiz. **46**, 1823 (1964) [Sov. Phys. JETP **19**, 1228 (1964)].
- [12] C. J. Lambert and R. Raimondi, J. Phys.: Condens. Matter **10**, 901 (1998).
- [13] G. E. Blonder, M. Tinkham, and T. M. Klapwijk, Phys. Rev. B **25**, 4515 (1982).
- [14] J. C. Cuevas, A. Martín-Rodero, and A. L. Yeyati, Phys. Rev. B **54**, 7366(1996).
- [15] C. W. J. Beenakker, Phys. Rev. B **46**, 12841 (1992).
- [16] Q. -f. Sun, J. Wang, and T. -h. Lin, Phys. Rev. B **59**, 3831 (1999).
- [17] The limit $eV \rightarrow \infty$ after $\Delta \rightarrow \infty$ means $\Delta \gg eV \gg |E_0|, L, R$.
- [18] M. Büttiker, Phys. Rev. B **46**, 12485 (1992).
- [19] V. T. Petrashov *et al.*, Phys. Rev. Lett. **74**, 5268 (1995).
- [20] E. Toyoda, H. Takayanagi, H. Nakano, *et al.*, Phys. Rev. B. **59**, R11653 (1999).

FIGURE CAPTIONS

Fig. 1 Schematic diagram of the hybrid N/S interferometer. Below is the illustration of several AR processes: (a) is the resonant AR through N-QD-S, (b) is the nonresonant AR through N-I-S, and (c) is the cross AR between N-QD-S and N-I-S.

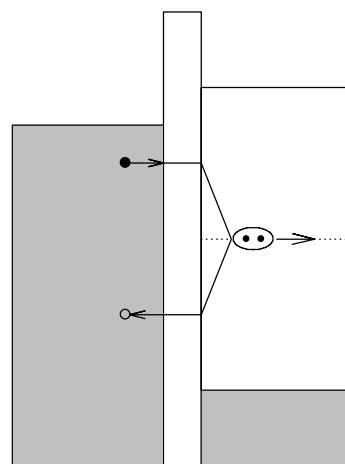
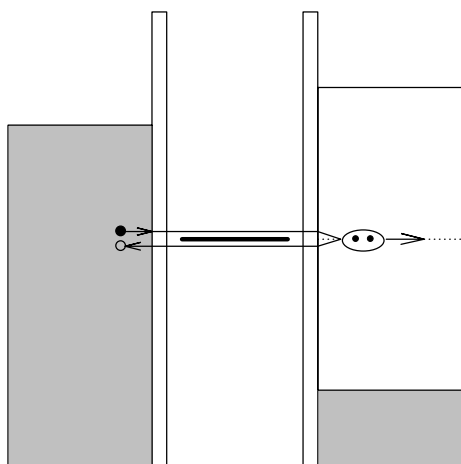
Fig. 2 Linear and nonlinear transport through (a) N-(I,QD)-S and (b) N-(I,QD)-N, with vanishing AB phase. For clarity, the background current through the reference arm N-I-S or N-I-N has been subtracted from the total current. The background transmission probability T_b is chosen as 0 (solid), $\frac{1}{4}$ (dot), $\frac{1}{2}$ (dash), $\frac{3}{4}$ (dot), 1 (solid), with the symmetric coupling strengths $L = R$.

Fig. 3 Phase dependence of the N-(I,QD)-S interferometer. The left panel shows the curves of G vs E_0 and I vs E_0 for $T_b = \frac{1}{2}$, with fixed AB phase $\phi = 0$ (solid), $\frac{\pi}{4}$ (dash), and $\frac{\pi}{2}$ (dot). The right panel shows the curves of G vs ϕ and I vs ϕ at the selected points marked in the left curves.



(a) N - QD - S

(b) N - I - S



(c1) N - QD - S

(c2) N - I - S

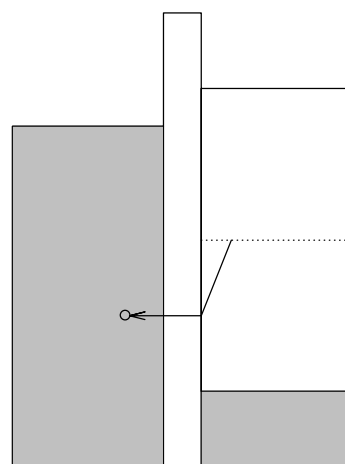
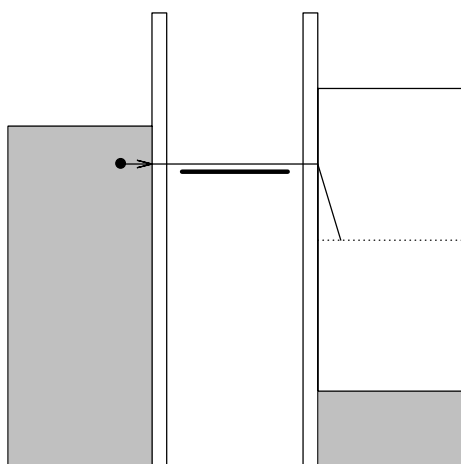


Fig.1

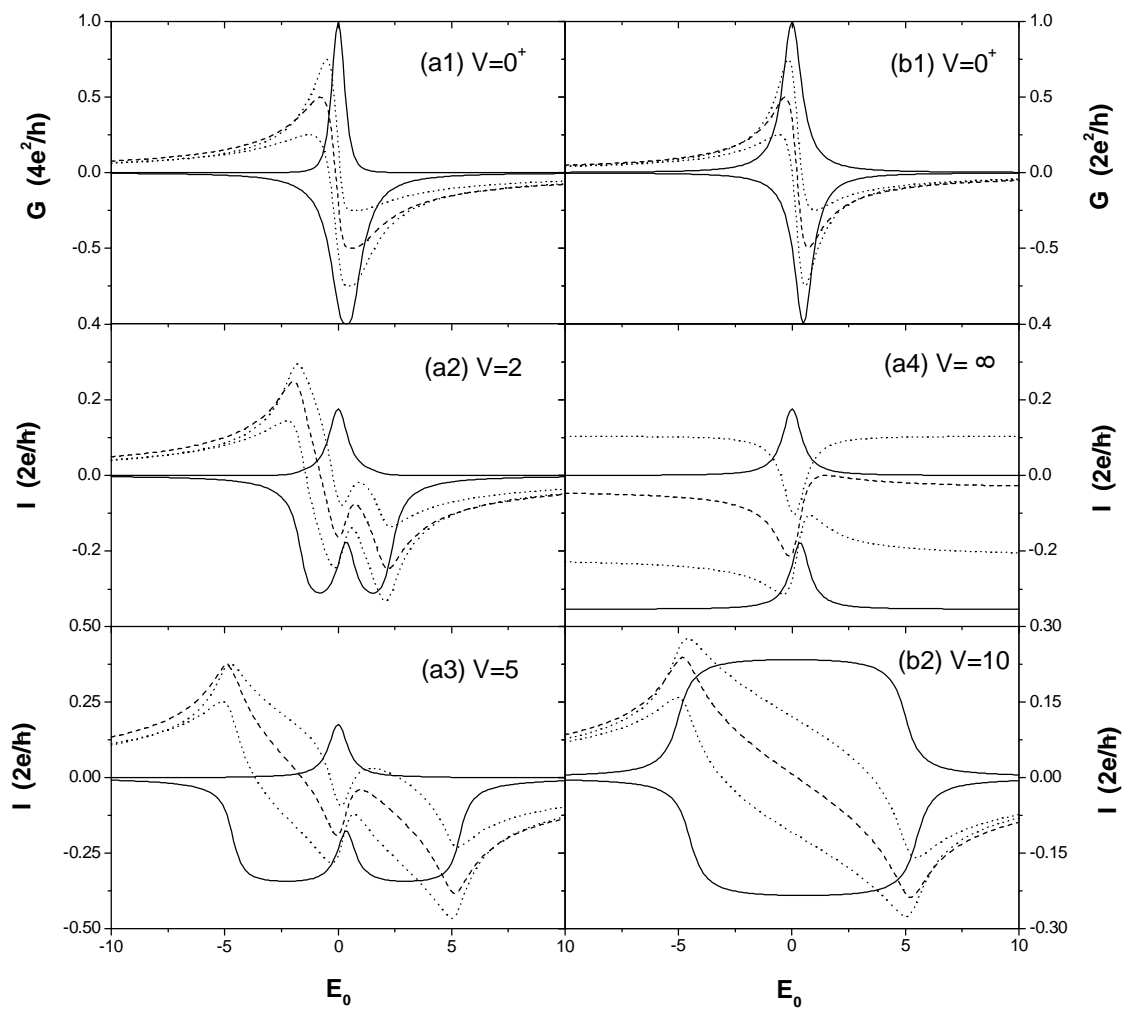


Fig.2

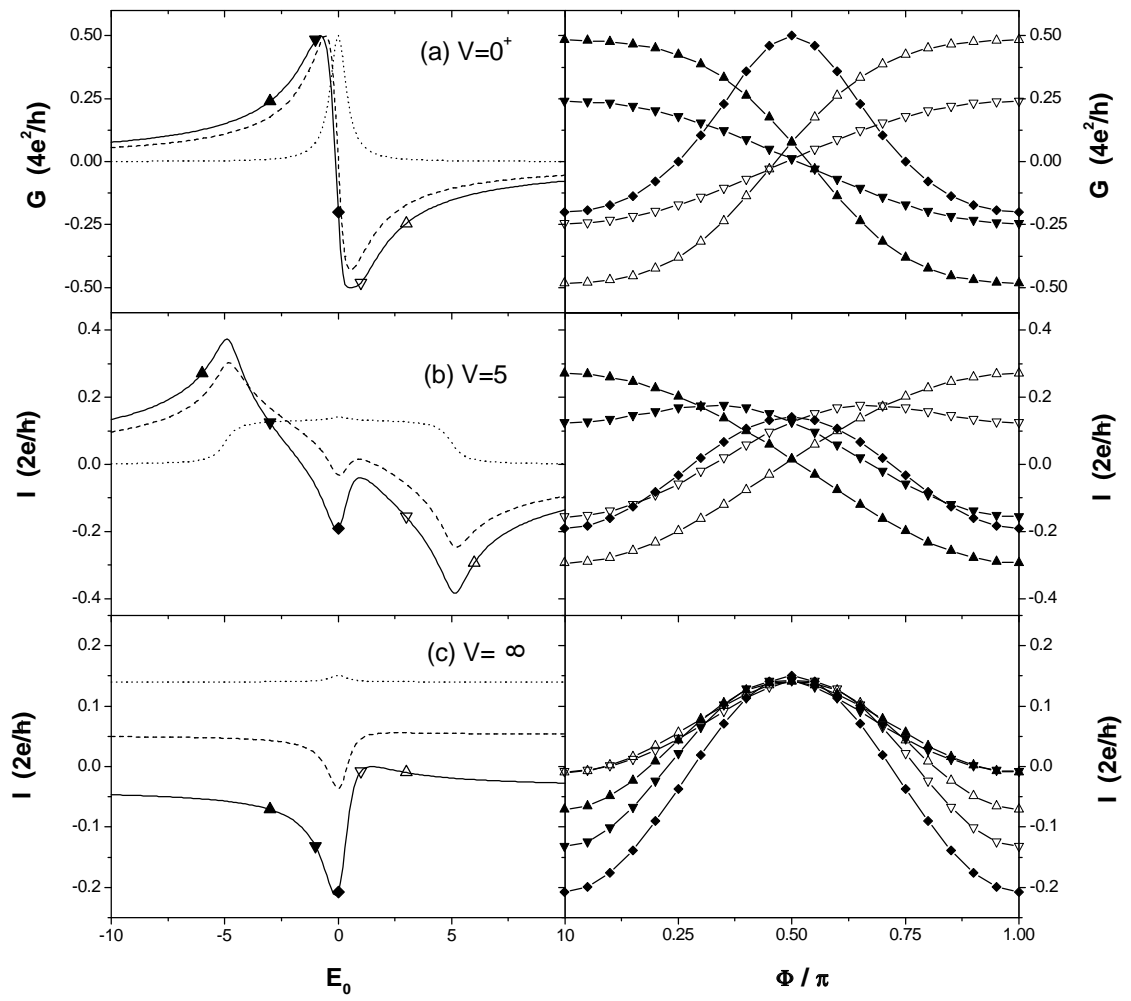


Fig.3